

Potential Vorticity Diagnosis of the Severe Convective Regime. Part IV: Comparison with Modeling Simulations of the Moore Tornado Outbreak

DAVID A. GOLD* AND JOHN W. NIELSEN-GAMMON

Department of Atmospheric Sciences, Texas A&M University, College Station, Texas

(Manuscript received 16 November 2006, in final form 25 June 2007)

ABSTRACT

A potential vorticity (PV) diagnostic framework is used to explore the sensitivity of the 3 May 1999 Oklahoma City tornado outbreak to the strength of a particular PV anomaly proximate to the geographical region experiencing the tornado outbreak. The results derived from the balanced PV diagnosis agree broadly with those obtained previously in a numerical simulation of the same event, while offering additional insight into the nature of the sensitivity. Similar to the findings of other cases, the balanced diagnosis demonstrates that intensifying (removing) the PV anomaly of interest increases (decreases) the balanced CAPE over the southwestern portion of the outbreak region, reduces (increases) the storm-relative helicity, and increases (reduces) ascent. The latter finding, coupled with the results of the modeling study, demonstrates that intensifying a PV anomaly proximate to an outbreak environment can increase the likelihood that more widespread and possibly less tornadic convection will ensue. The overall results of the balanced diagnosis complement those of other case studies, leading to the formulation of a conceptual model that broadly anticipates how the convective regime will respond to changes in intensity of upper-tropospheric weather features.

1. Introduction

One of the most devastating tornadoes in Oklahoma state history occurred on 3 May 1999 (hereafter referred to as the “Moore outbreak”). This event was part of a tornado outbreak that produced a total of 66 tornadoes over Oklahoma and Kansas (Speheger et al. 2002). The lack of clearly identifiable mesoscale forcing mechanisms and the widespread presence of atmospheric conditions highly supportive of tornadic supercells suggest that this event was governed at least in part by the large-scale environment (Thompson and Edwards 2000).

In an effort to determine the roles that the upper-tropospheric potential vorticity (PV) distribution played in regulating the outbreak, Roebber et al. (2002, hereafter RSR02) perform a multiple-resolution modeling study of the Moore outbreak to explore the sensitivity of the mode, intensity, and distribution of con-

vection to a specific PV anomaly that approached the southern portion of the outbreak area. The existence of a modeling study examining the role of the upper-level PV in regulating the convective outbreak affords a unique opportunity for comparison with the PV modification and inversion technique developed in Gold and Nielsen-Gammon (2008a,b) and Nielsen-Gammon and Gold (2008, hereafter Parts I, III, and II, respectively). The primary purpose of this paper is to compare the results gained from the balanced diagnosis used in the current work against the full-scale modeling investigation of the same case by RSR02. While the balanced diagnosis cannot include fundamentally unbalanced processes or interactions and feedbacks that evolve through time, most of the results of the balanced diagnosis agree qualitatively with the model-derived diagnoses performed by RSR02. Moreover, the balanced diagnoses will afford physical insights complementary to those offered in the modeling study.

A second purpose of this paper is to use a second case study to investigate the extent to which the insights gleaned from the case diagnosed in Part III represent general characteristics of the sensitivity of the severe convective regime (SCR) to changes in the strength of upper-level mobile troughs. To the extent that the re-

* Current affiliation: PPM Energy, Inc., Houston, Texas.

Corresponding author address: David A. Gold, P.O. Box 420898, Houston, TX 77242.
E-mail: dr_david_gold@earthlink.net

sults from Parts III and the current paper are general, it is possible to create a conceptual model that describes how upper-level mobile trough errors can be expected to alter the SCR and to apply that model to future forecasting scenarios.

The current paper is organized as follows: an overview of the RSR02 findings is presented in section 2 followed by the balanced diagnoses in section 3. The two sets of results are compared in section 4 and a discussion of the results and conclusions stemming from both case studies (Hesston in Part III and Moore in the current paper) is given in section 5, along with possibilities for further work.

2. An overview of the RSR02 modeling results

A comparison of results here to those of RSR02 will be facilitated by summarizing the findings of the latter study. RSR02 test the sensitivity of the Moore convective environment and storm evolution to the existence of a specific PV anomaly by altering the PV distribution of the model's initial conditions (ICs). First, RSR02 perform a control run (CNTL) of a nested version of the fifth-generation Pennsylvania State University–National Center for Atmospheric Research Mesoscale Model (MM5; Dudhia 1993) encompassing North America in the outermost nest and the entire convective outbreak region within the inner nests. The finest nested resolution is a 2-km grid spacing with 23 vertical levels. The CNTL run is shown to produce a realistic simulation of the upper-level PV distribution (RSR02, their Fig. 3) as well as of the distribution of upper-tropospheric cirrus clouds, surface winds, and dry-line position (RSR02, their Fig. 6), all features relevant to the Moore convective evolution and forecast. However, the details of the convective simulation were not well forecast, with the positions of the simulated storms being displaced southward from their observed locations by several hundred kilometers (RSR02, their Fig. 5).

The PV anomaly selected by RSR02 for the sensitivity analysis is one initialized just off the southern California coast at 0000 UTC 3 May 1999 [the “southern anomaly” (SA); Fig. 1]. Removal of the SA [their no PV (NOPV) experiment; Fig. 2] is accomplished by subtracting from the model's initialization the balanced flow perturbation associated with the SA and obtained via the Davis and Emanuel (1991) piecewise PV inversion technique. A doubling of the SA (producing their 2XPV experiment; Fig. 3) is accomplished by adding the balanced flow perturbation to the initialization. The SA itself is defined relative to a time-mean state.

RSR02 test the sensitivity of the following aspects of the outbreak to the removal or doubling of the SA: the

mode, severity, and spatial coverage of convection; the amount of cirrus clouds, posited to reduce heating and thereby delay and restrict convective initiation; and the magnitude of the convective parameter values across the outbreak region, specifically CAPE, bulk Richardson shear (BRNSHR), and 0–3-km storm-relative environmental helicity (SREH; Davies-Jones 1984). Convective intensity and coverage, as well as the amount of cirrus present in the simulation, are related to the strength of the forced ascent, which RSR02 examine by computing the advection of tropopause pressure, p_{tr} . The stronger forcing associated with 2XPV is found to result in a greater number and coverage of convective cells, with a much more expansive cirrus canopy [whose contribution to delayed convective inhibition (CIN) removal through damping of insolation is offset by the increased forcing for ascent]. Removal of the SA (NOPV) reduces the overall coverage of convective storms, but the few updrafts that do form are more intense and longer lived than those produced by 2XPV.

The environmental convective parameters are also found to exhibit some sensitivity to the details of the SA (Fig. 4). Modifying the SA is found to significantly change the vertical shear parameters, with BRNSHR and SREH significantly reduced (increased) in the 2XPV (NOPV) simulation. CAPE is not found to change much in the 2XPV simulation, but is reduced east of the Oklahoma segment of the dryline, which is found to be displaced to the east relative to CNTL. The combination of decreased vertical shear and SREH along with increased forcing for ascent present in the 2XPV simulation were cited by the authors as contributing to the reduced intensity and enhanced spatial coverage of the convection in that run and vice versa in the NOPV simulation.

The numerical simulations of RSR02, while revealing the potential impacts that a change to the SA might have on the convective regime, did not provide physical insights into every aspect of the sensitivity. For example, RSR02 speculate that subtle interactions between the SA and a separate PV anomaly situated farther to its northwest [the northern anomaly (NA)] are responsible for dramatically reducing (increasing) BRNSHR and SREH in the 2XPV (NOPV) case. The balanced diagnosis presented below, however, reveals that a stronger SA results in PV contours that are more meridionally oriented, thereby rotating the deep-layer shear vector and storm motion vector (SMV) counterclockwise and reducing the SREH and BRNSHR.

3. Balanced diagnosis of the Moore case

The procedures for performing the balanced diagnosis are described in Part I. Briefly, gridded reanalysis

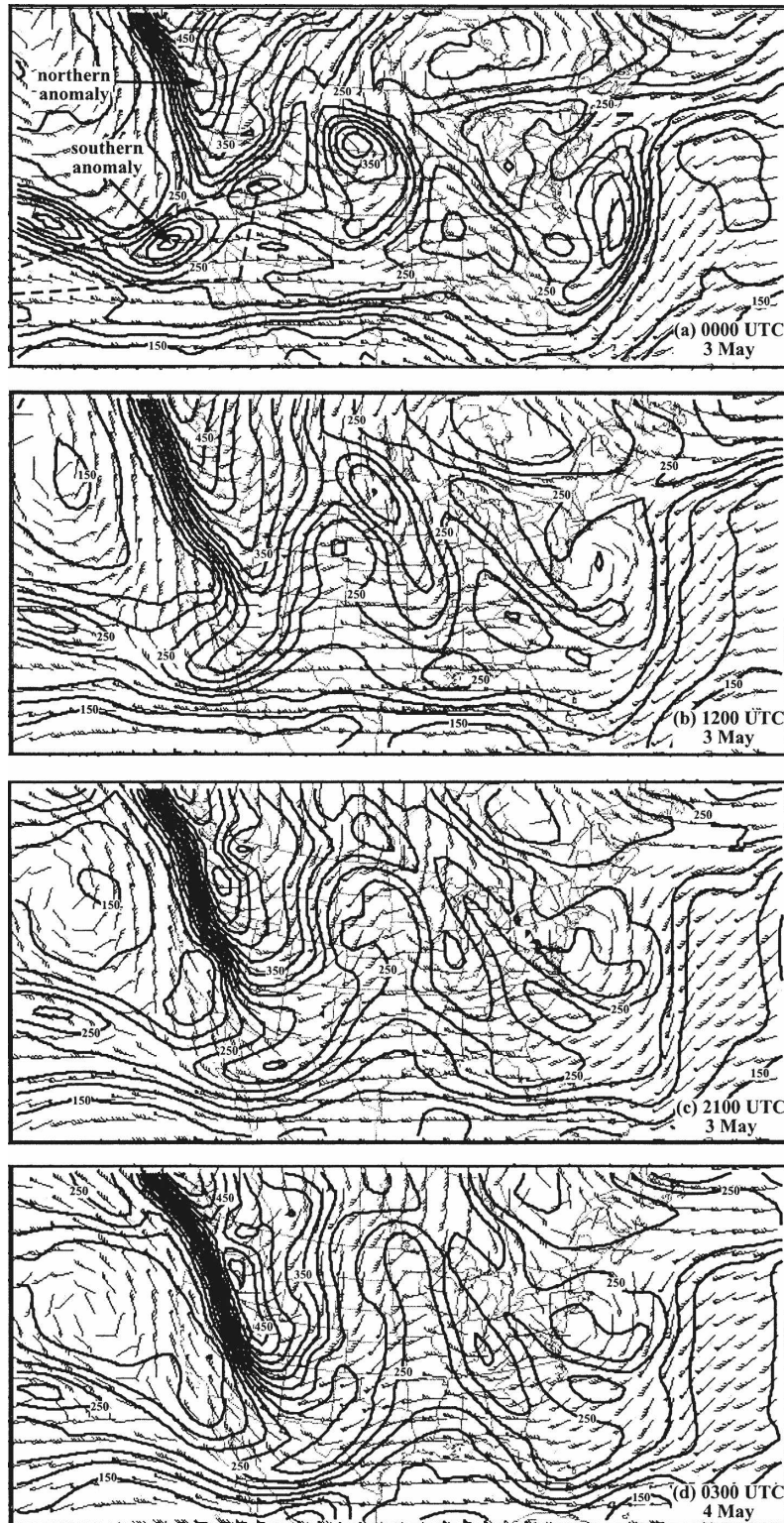


FIG. 1. Pressure (contour interval 25 hPa) and wind on the dynamic tropopause derived from RSR02 CNTL. The dynamic tropopause is defined as the 1.5-PVU surface ($1 \text{ PVU} = 1 \times 10^{-6} \text{ m}^2 \text{ K s}^{-1} \text{ kg}^{-1}$). Wind barbs are plotted according to the standard meteorological convention (pennant, 25 m s^{-1} ; long barb, 5 m s^{-1} ; short barb, 2.5 m s^{-1}): (a) 0000 UTC 3 May 1999, the dashed triangle over the Pacific Ocean encloses the area selected as the SA for PV modification purposes by RSR02; (b) 1200 UTC 3 May; (c) 2100 UTC 3 May; and (d) 0300 UTC 4 May 1999. From RSR02.

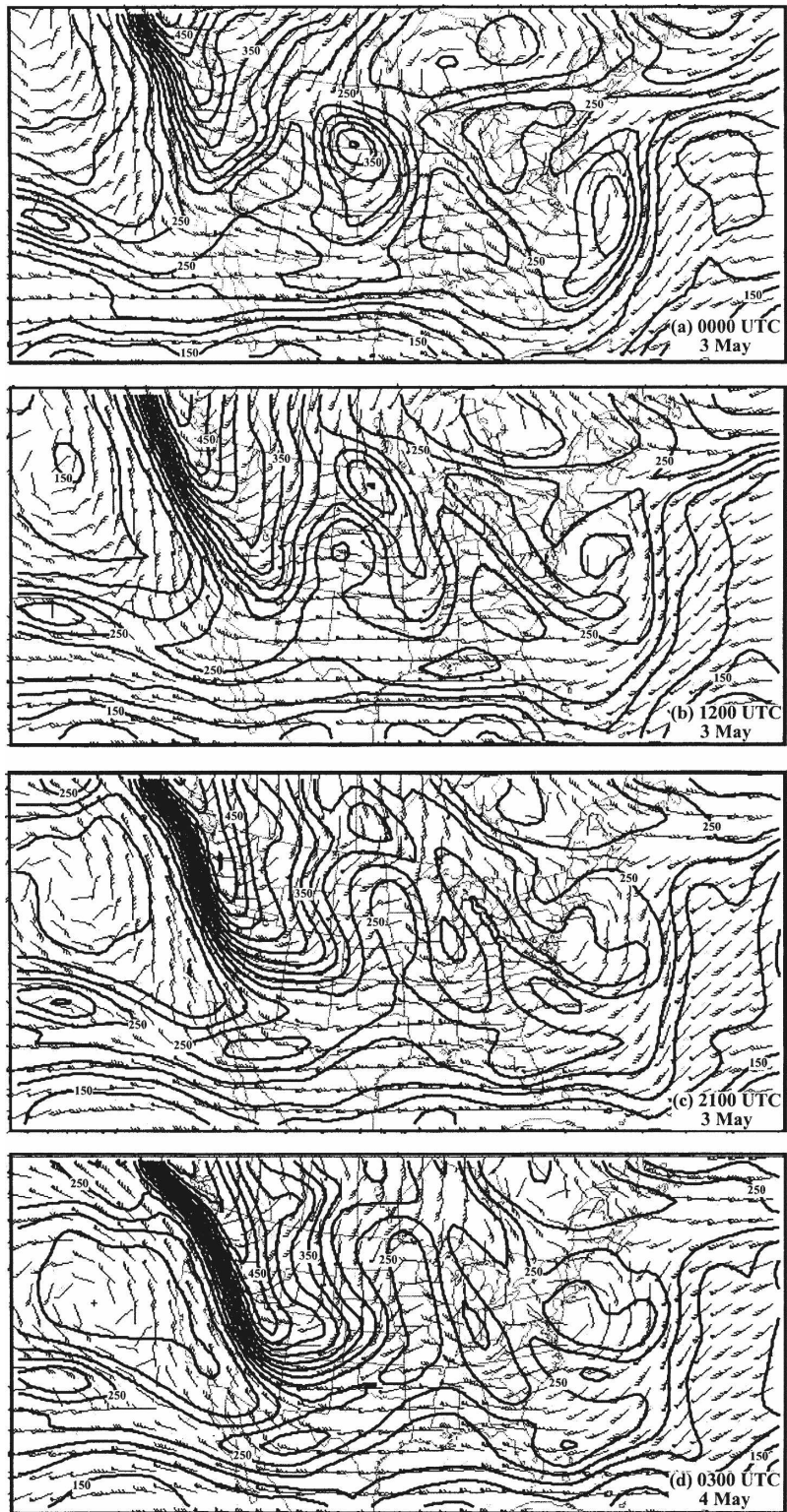


FIG. 2. Same as in Fig. 1 but derived from the forecast with the SA removed (NOPV). From RSR02.

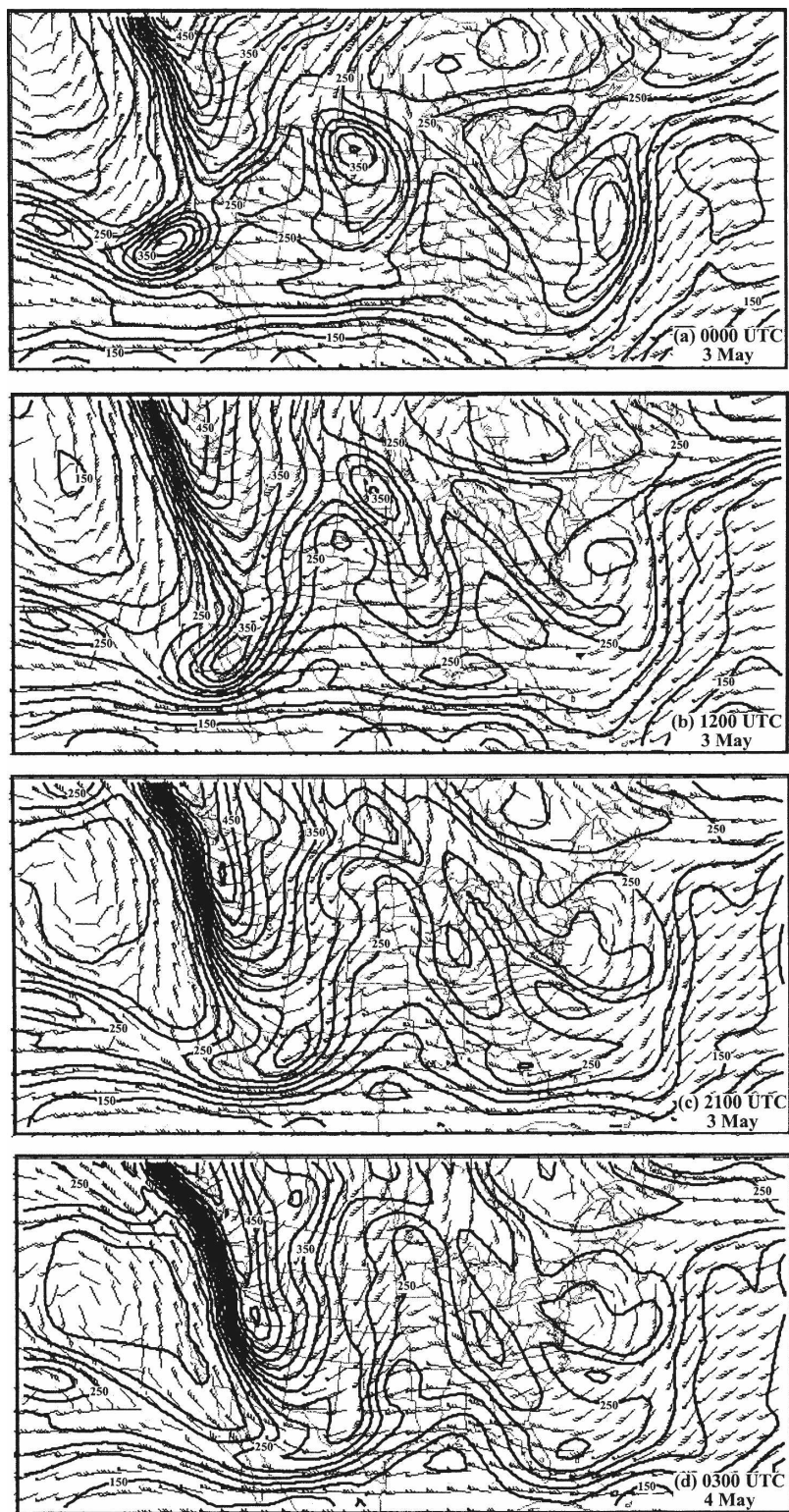


FIG. 3. Same as in Fig. 1 but derived from the forecast with the SA doubled (2XPV). From RSR02.

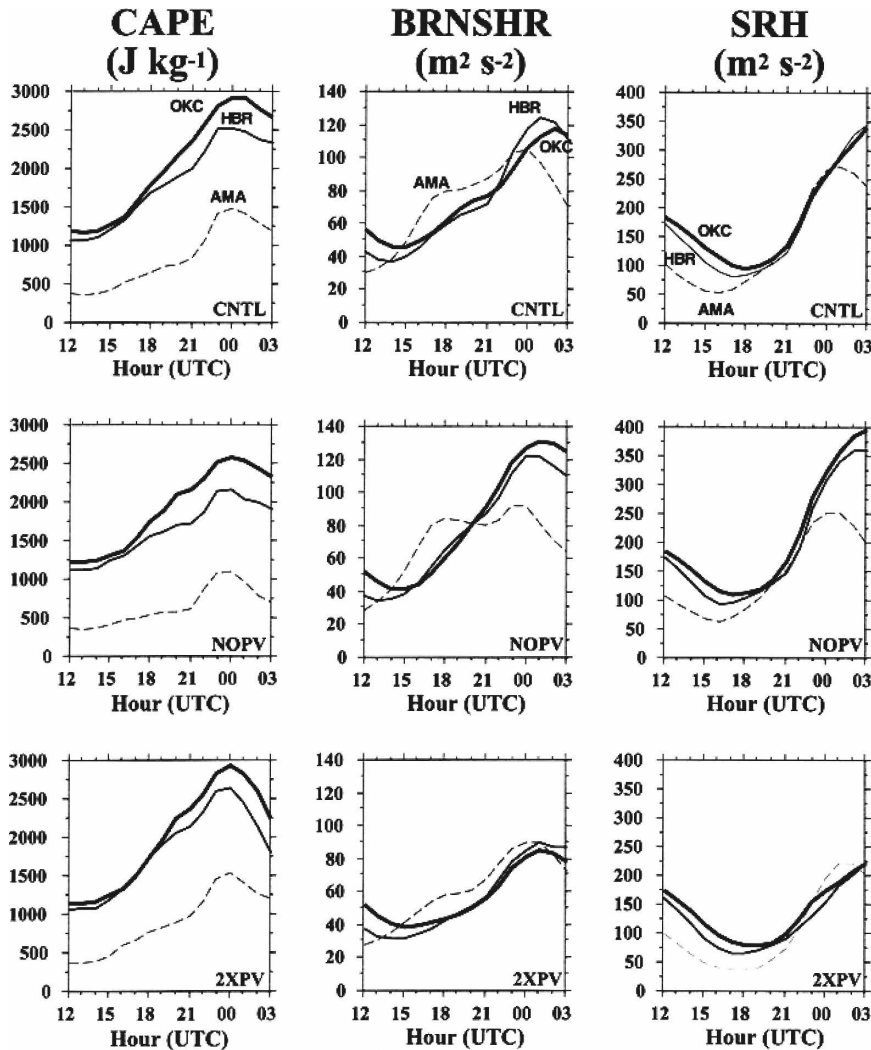


FIG. 4. Time series of CAPE (J kg^{-1}), BRNSHR ($\text{m}^2 \text{s}^{-2}$), and SREH ($\text{m}^2 \text{s}^{-2}$) for 1200 UTC 3 May–0300 UTC 4 May 1999 for CNTL, NOPV, and 2XPV. Measures are computed within $216 \text{ km} \times 216 \text{ km}$ boxes centered on grid points corresponding to the positions of Amarillo (dashed), Hobart (solid), and Oklahoma City (thick solid). From RSR02.

data (Kalnay et al. 1996) are interpolated to a regular grid and extrapolated below ground to 1000 hPa. The PV inversion uses the time-dependent nonlinear balance equations (Davis and Emanuel 1991) for recovery of both nondivergent and irrotational winds. The PV modification, or surgery, algorithm is designed to produce realistic PV modifications and is controlled by specification of an amplitude, location, size, and shape. CAPE is computed (using surface parcels) from the inverted fields, while shear parameters are computed using the full winds modified by differences between the balanced state and the modified balanced state.

Corollary “experiments” are performed within the balanced framework by identifying and altering the SA in a manner analogous to the 2XPV and NOPV experi-

ments. The PV modification procedure described in Part I is used to both remove and amplify the PV associated with the SA at the following dates and times: 1200 UTC 3 May, 1800 UTC 3 May, and 0000 UTC 4 May 1999. Hereafter, the year, month, and day are omitted from times referenced in the discussion and it should be understood that 1200 UTC and 1800 UTC are on 3 May and 0000 UTC is on 4 May.

The PV anomaly to be altered is shown at 1200 UTC in Fig. 5a (enclosed by dashed box) and is represented in terms of the pressure on the dynamic tropopause, p_{tr} , to be consistent with Figs. 1–3. At 1800 UTC this feature moves eastward and appears to begin splitting into two “pieces,” a northern PV anomaly and a southern one, each of which is highlighted by the boxes in Fig. 5b.

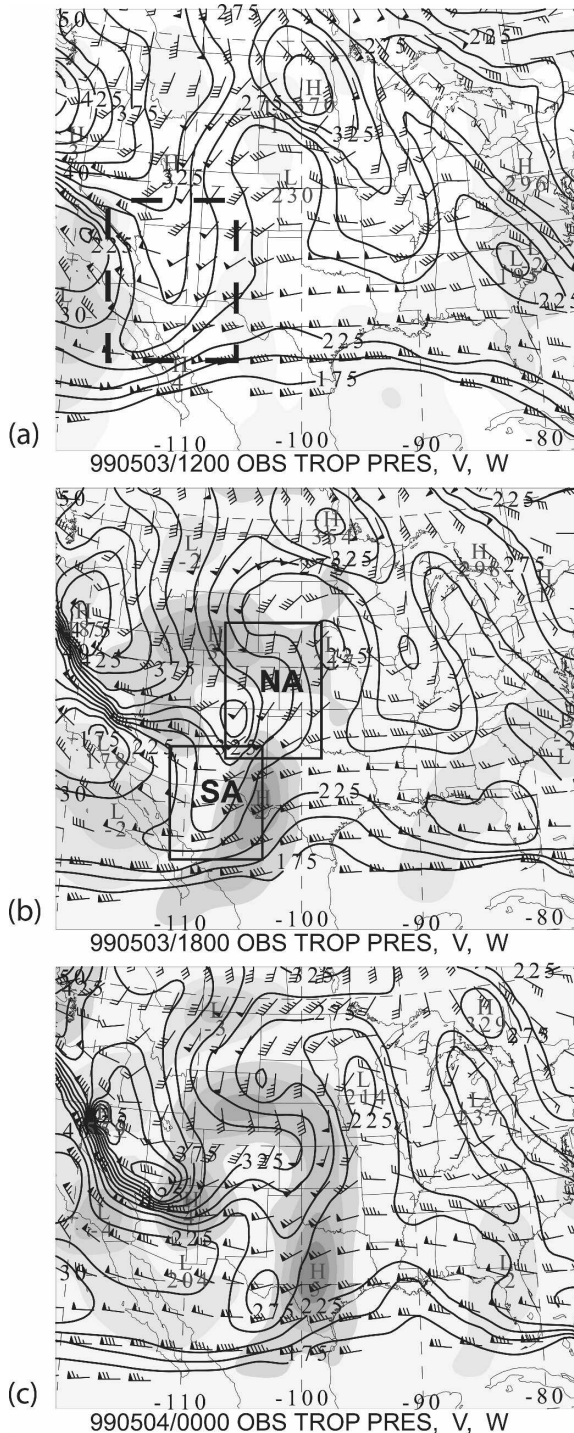


FIG. 5. Evolution of pressure (contoured every 25 hPa) and wind on the dynamic tropopause (1.5-PVU surface) computed from the reanalysis data; also plotted: vertical motion (at 500 hPa) on 3 May 1999. Wind barbs are plotted in knots (pennant, 50 kt; long barb, 10 kt; short barb, 5 kt). Vertical motion is shaded (cm s^{-1}): (a) 1200 UTC 3 May, the dashed box encloses the PV anomaly removed by RSR02 (see text for explanation); (b) 1800 UTC 3 May, the SA and NA are labeled and enclosed by solid boxes; and (c) 0000 UTC 4 May.

TABLE 1. PV modification parameters used to amplify (PVADD) and eliminate (PVSUB) the SA at the three times shown, using the PV modification technique described in Part I.

PV modification parameters for the 3 May 1999 case							
	Time	x_0	y_0	AMP	ϕ	a	b
PVADD	1200 UTC	30.0°N	100.00°W	0.6	$\pi/6$	4	6
	1800 UTC	30.0°N	107.50°W	0.7	0	4	6
	0000 UTC	32.5°N	102.50°W	0.6	$\pi/6$	5	6
PVSUB	1200 UTC	32.5°N	111.25°W	-0.6	$\pi/6$	4	6
	1800 UTC	32.5°N	107.50°W	-0.6	0	4	6
	0000 UTC	32.5°N	102.50°W	-0.6	$\pi/6$	5	6

The NA, which represents the easternmost extent of the larger-scale parent anomaly centered farther upstream, is manifested as a convex series of p_{tr} contours extending to central Kansas. The SA approaches western Texas at 1800 UTC, forcing synoptic-scale ascent over far western Texas and northern Mexico. By 0000 UTC, at which time the tornado outbreak is in progress, both PV anomalies have progressed eastward and the associated PV advection forces ascent along a broad swath to the east of the p_{tr} gradient (Fig. 5c).

The SA is modified at the three analysis times using the PV modification parameters presented in Table 1. Removal of the SA at each analysis time (the corollary to NOPV and hereafter referred to as PVSUB to distinguish the diagnosis from the simulation) is accomplished by selecting negative values of the amplification exponent A .

The corollary to 2XPV, amplification of SA (hereafter referred to as PVADD) is achieved by choosing positive values of A . The p_{tr} distributions associated with the PVADD (Fig. 6) and PVSUB (Fig. 7) transformations are to be compared with RSR02's 2XPV (Fig. 3) and NOPV (Fig. 2) simulations. For brevity of reference, the unaltered atmospheric fields will hereafter be referred to as ORIG (the analyzed counterpart to RSR02's CNTL).

Pressure, anomalous balanced wind, and anomalous vertical motion on the tropopause associated with the amplified SA (PVADD) are presented in Fig. 6. Ascent is increased relative to ORIG over western Texas by 1800 UTC (Fig. 6b) and even more so across southern and central Texas by 0000 UTC, with peak values 2 cm s^{-1} greater than diagnosed in ORIG (Fig. 6c). The amplified SA is also associated with a cyclonic balanced wind anomaly and an increased southerly balanced wind component across Texas and Oklahoma by early evening. The enhanced southerly balanced wind component contributes to a backed SMV and reduced SREH over Oklahoma and southern Kansas, with

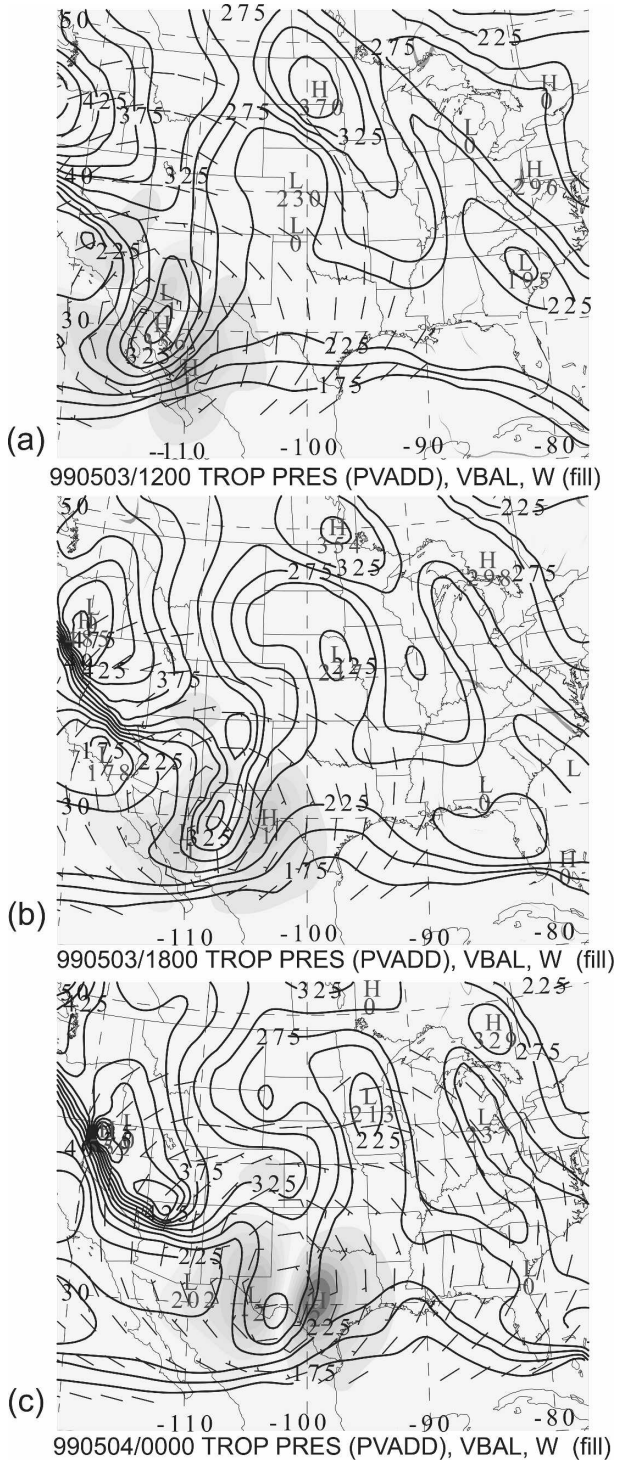


FIG. 6. Same as Fig. 5 but obtained from PVADD diagnosis. The wind barbs are those of the balanced wind (nondivergent plus irrotational) difference between ORIG and PVADD. The shading corresponds to the vertical motion difference between the two diagnoses. Peak positive vertical velocity perturbations, corresponding to enhanced ascent, occur east of the SA at all times, with values ranging from 1 cm s^{-1} at 1200 UTC to 2 cm s^{-1} at 0000 UTC.

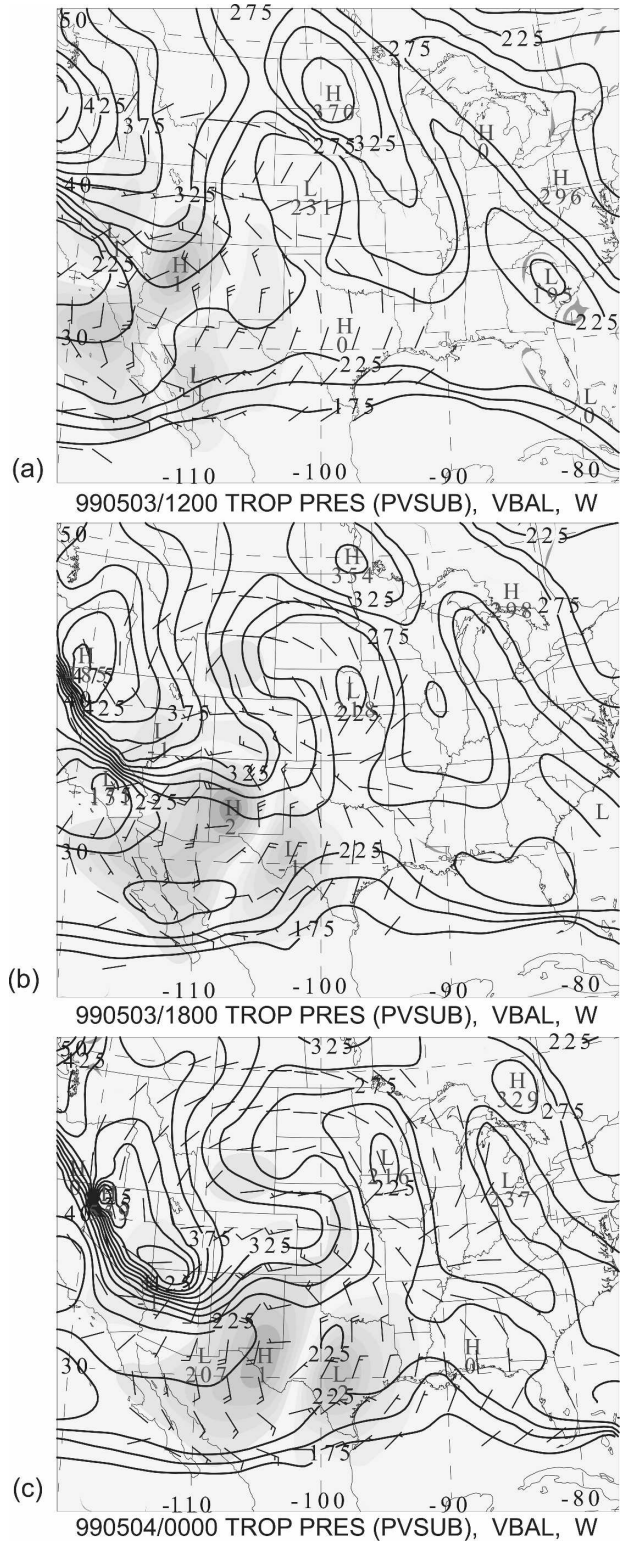


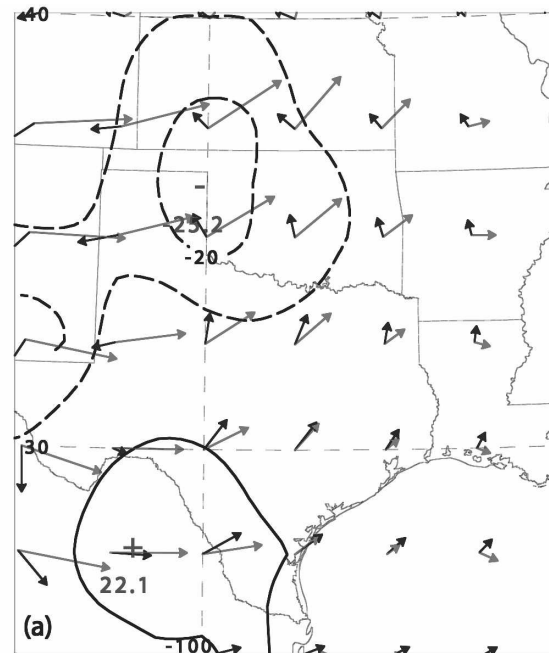
FIG. 7. Same as in Fig. 6 but obtained from PVSUB diagnosis.

SREH values $10\text{--}20\text{ m}^2\text{ s}^{-2}$ less than observed (reduced by 5%–10%) over this region by 0000 UTC (Fig. 8a). PVADD increases the CAPE across western Texas northward into the Texas Panhandle and western Oklahoma, with peak increases of nearly 350 J kg^{-1} diagnosed across western Texas by 0000 UTC (Fig. 8b). Most of the CAPE change occurs along and behind the dryline, whose approximate subjectively analyzed position is shown. Both the magnitude and sign of the convective parameter changes associated with PVADD agree with those produced by a similar PV amplification experiment (AMP) in the Hesston case (Part III), with the exception of the vertical velocity perturbations, which are considerably stronger in the Moore case than those diagnosed in Hesston. The similarity between the results of the balanced diagnosis in the two cases is obtained despite differences in the location and strength of the PV modifications induced, as well as differences in the background environments.

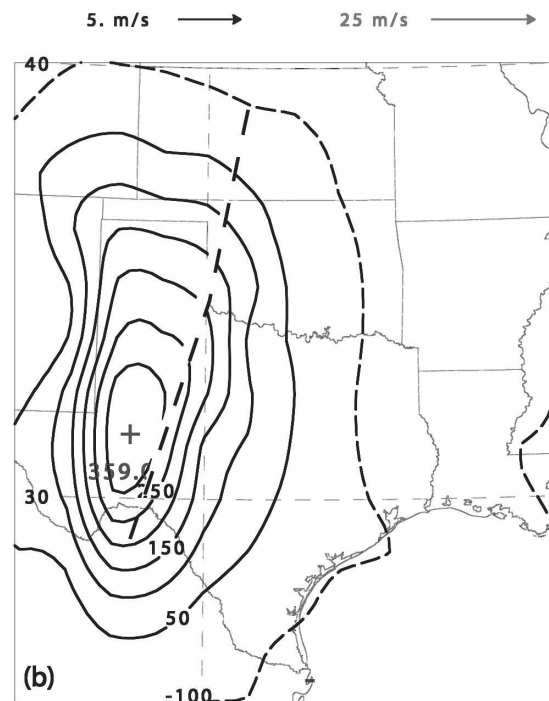
Removing the SA (Fig. 7) decreases the ascent over Texas by the afternoon and early evening of 3 May in the same location experiencing increased upward motion in PVADD. Ascent is reduced by nearly 2 cm s^{-1} over southwestern Texas at 0000 UTC. The PVSUB balanced fields also feature an anticyclonic wind anomaly that translates eastward during the analysis period, inducing an increased northerly wind component over the southern plains and enhanced westerly balanced winds over Kansas and Nebraska by 0000 UTC. The resulting SMVs are veered over much of the outbreak region relative to those associated with the unmodified PV in ORIG (Fig. 9a), yielding SREH values $10\text{--}20\text{ m}^2\text{ s}^{-2}$ higher than the ORIG field over western and central Kansas and Oklahoma. The NOPV CAPE is significantly reduced compared to ORIG across most of Texas, Oklahoma, and Kansas (Fig. 9b), with values reduced by as much as 350 J kg^{-1} over western Texas immediately east of the dryline. Once again, these results agree qualitatively and quantitatively with those of the Hesston diagnosis (Part III).

The spatial relationships between SREH and shear changes attributable to the PVADD and PVSUB experiments, depicted in Fig. 10, are more complicated than in the Hesston case (refer to Part III, their Figs. 8b, 12b), where SREH and shear alterations are everywhere roughly 90° out of phase.

In both cases (Hesston and Moore), the shear anomalies are located on the cross-shear flanks (relative to the background shear vector) of the PV anomalies. In fact, this will be true of *any* case where the background shear is fairly uniform across a nearly circular balanced flow perturbation associated with a PV anomaly (although upper-level fronts or other meso-

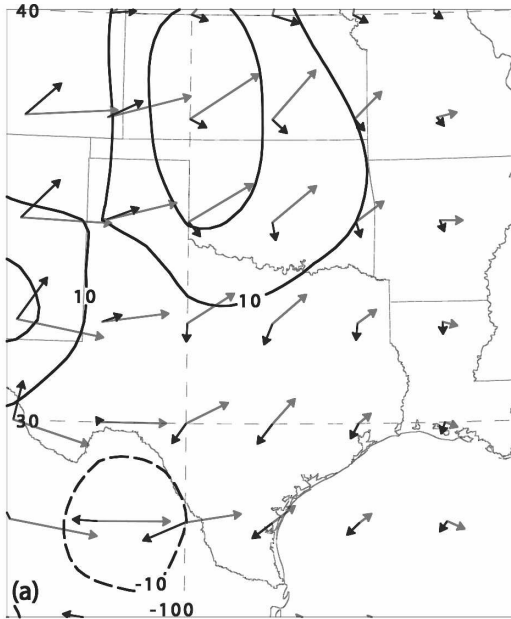


990504/0000 SREHMOD-SREH (PVADD), SMV CHANGE

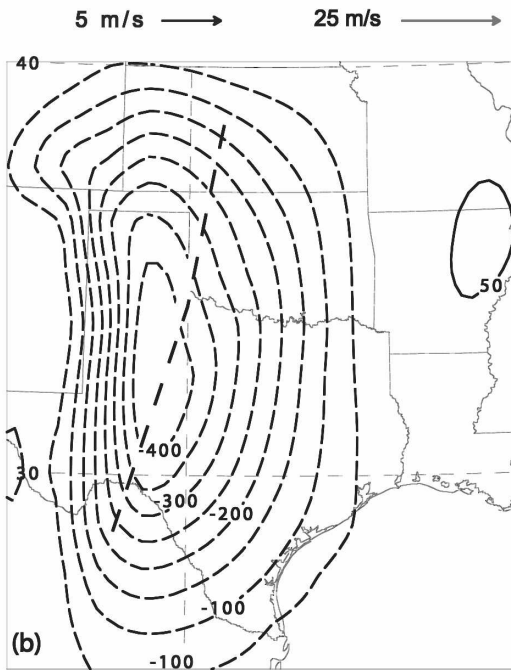


990504/0000 CAPEMOD-CAPE (PVADD)

FIG. 8. Difference in the 3 May 1999 convective parameters between the PVADD and ORIG diagnoses: (a) difference in 0–3-km SREH (contoured every $10\text{ m}^2\text{ s}^{-2}$, negative values dashed), Bunkers SMVs (gray colored arrows, m s^{-1} with vector scale shown below figure), and difference in SMVs (black arrows); (b) difference in balanced CAPE (contoured every 50 J kg^{-1}), with approximate position of the surface dryline (from observations) demarcated by the thick black dashed line.



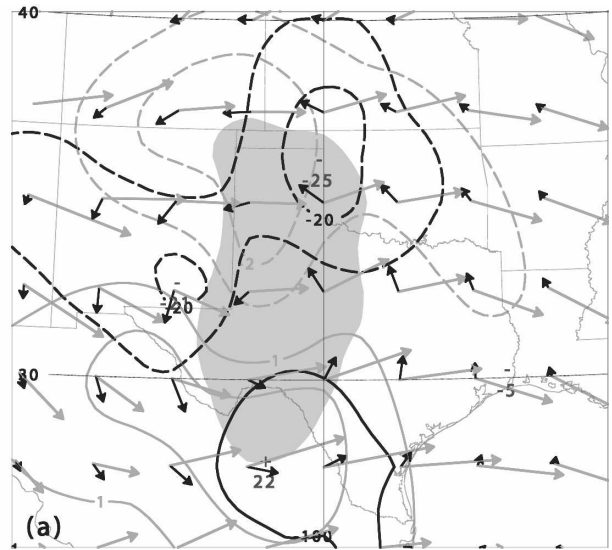
990504/0000 SREHMOD-SREH (PVSUB), SMV CHANGE



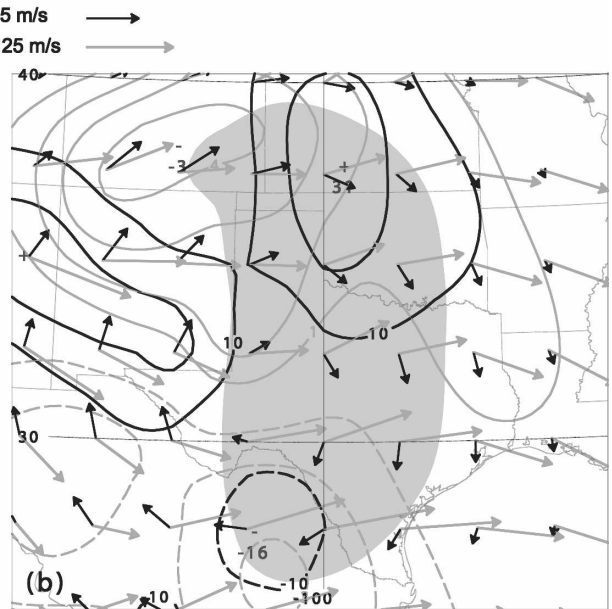
990504/0000 CAPEMOD-CAPE (PVSUB)

FIG. 9. Same as in Fig. 8, but for the difference in the diagnosed convective parameter fields between PVSUB and ORIG.

scale features may complicate this shear anomaly pattern). The SREH dipole is oriented primarily in the cross-shear direction in the Moore case, as opposed to the alongshear direction in the Hesston case. Exploring the reasons for this difference are beyond the scope of



990504/0000 SREH vs SHEAR



990504/0000 SREH vs SHEAR

FIG. 10. SREH anomalies ($\text{m}^2 \text{s}^{-2}$, black contours), 0–6-km shear anomalies (m s^{-1} , gray contours), shear vectors associated with the full analyzed winds (gray arrows), perturbation winds (black arrows), and CAPE anomalies (gray shading) at 0000 UTC 4 May 1999 for (a) PVADD and (b) PVSUB. The shaded gray regions denote the area where perturbation CAPE is (a) greater than 100 J kg^{-1} and (b) less than -100 J kg^{-1} . Contour interval for SREH is $10 \text{ m}^2 \text{ s}^{-2}$ in both (a) and (b); contour interval for shear is 1 m s^{-1} in (a) and 2 m s^{-1} in (b). Vector scale, shown between (a) and (b), is exaggerated for the perturbation shear vectors and mitigated for the background shear vectors.

the current work. However, it is notable that as in the Hesston case, SREH is reduced downshear for the PV amplification and increased downshear for the PV reduction. An examination of other cases where the CAPE-bearing region is characterized by little along-stream variation in shear reveals the same spatial relationships (not shown) as those demonstrated in the Hesston and Moore cases presented here.

4. Comparing the diagnosed and simulated results

RSR02 analyze time series of p_{tr} advection derived from the CNTL, 2XPV, and NOPV simulations at various locations (RSR02, their Fig. 14) to deduce the dependence of forcing on the SA anomaly amplitude. In NOPV, the peak positive advectons (forcing for ascent) are weaker and occur somewhat earlier than in CNTL and are primarily associated with the NA, while in 2XPV, peak advectons are greater in magnitude, somewhat delayed, and are attributable to the strengthened SA. The diagnosed vertical motion fields, presented in Fig. 6 (PVADD) and Fig. 7 (PVSUB), generally corroborate the findings derived from the modeled forcing fields: PVADD produces stronger ascent over Texas and PVSUB reduces the ascent there. However, there is no indication in the diagnosed vertical motion that ascent peaks over western Oklahoma at 1800 UTC close to the time when the NA-induced forcing is maximized there in the time series. An examination of the diagnosed p_{tr} advection (not shown) indicates that the strength of the forcing over western Kansas and western Oklahoma associated with the NA is very similar in PVSUB and PVADD, accounting for the lack of a difference between the corresponding diagnosed vertical motion fields there.

The increased 2XPV ascent inferred over Texas at 0000 UTC is hypothesized by RSR02 to explain the southward-displaced and predominantly linear convection simulated in that run compared with CNTL, which features more intense isolated supercells (as opposed to linear storms) occurring farther north. The PVADD diagnosis here produces a qualitatively similar vertical motion enhancement. The diminished ascent diagnosed over Texas in the PVSUB case at 0000 UTC (Fig. 7c) is also consistent with RSR02's NOPV simulations, in which the weaker forcing for ascent over the warm sector produces less overall convection, with a higher percentage of robust long-lived supercells than produced by the 2XPV run. The qualitative agreement between the RSR02 simulations and balanced diagnosis with regards to the sign and location of the forcing and associated vertical motion (with the exception of the differences noted above) suggests that it is possible to make

the same inferences regarding convective initiation and mode in each approach. Specifically, an amplified SA results in increased ascent over the southern portion of the outbreak region, which increases the probability that storms will become more widespread and possibly evolve more quickly into a linear configuration, especially if CIN is fairly weak over the area. Conversely, removing the SA will tend to reduce ascent over the southern portion of the outbreak region and thus lead to a higher chance that storms will be more isolated.

Aside from mentioning that SREH and BRNSHR differences are attributable to complex interactions between the NA and SA, RSR02 offer little physical insight into how the differences in PV between the two cases relate to the modeled changes in the vertical shear parameters. A key advantage of the balanced diagnostic framework is its ability to determine whether the link between changes in the PV distribution and corresponding changes in the vertical shear is a direct one or a consequence of a complex sequence of interactions. The southeastward extension of the NA is accentuated in RSR02's NOPV simulation (refer to their Fig. 12) and is restricted in the 2XPV run (refer to their Fig. 13), leading to decreased (increased) shear and SREH in the former (latter) case. The balanced diagnosis demonstrates that, as in the Hesston case, changing the PV associated with the SA leads to a change in the SMV and, therefore, the SREH (refer to Fig. 10). To better demonstrate the relationship between the PV distribution and its effect on shear-related parameters (SMV, BRNSHR, and SREH), the original and modified p_{tr} distributions are presented in Fig. 11, along with the shear vectors before and after the change. In PVADD (Fig. 11a), the total shear vector \mathbf{S} is shortened and rotated counterclockwise over Oklahoma and north Texas, whereas in PVSUB (Fig. 11b), \mathbf{S} is lengthened and rotated clockwise.

These changes in the total shear vector yield SMVs that are slightly to the left and shorter (right and longer) than the ORIG SMVs for the PVADD (PVSUB) experiment, thereby reducing (increasing) the SREH (refer to Fig. 10).

In the NOPV simulation, reductions in grid-averaged peak CAPE values are found at three sample locations along an east–west corridor extending from Amarillo, Texas, to Oklahoma City, Oklahoma (Fig. 4), the chief effect of eliminating the SA being to warm the air column in the area. This agrees with the finding of the PVSUB balanced diagnosis, which demonstrates that balanced CAPE is reduced substantially over western Texas, Oklahoma, and Kansas (refer to Fig. 9b) at 0000 UTC.

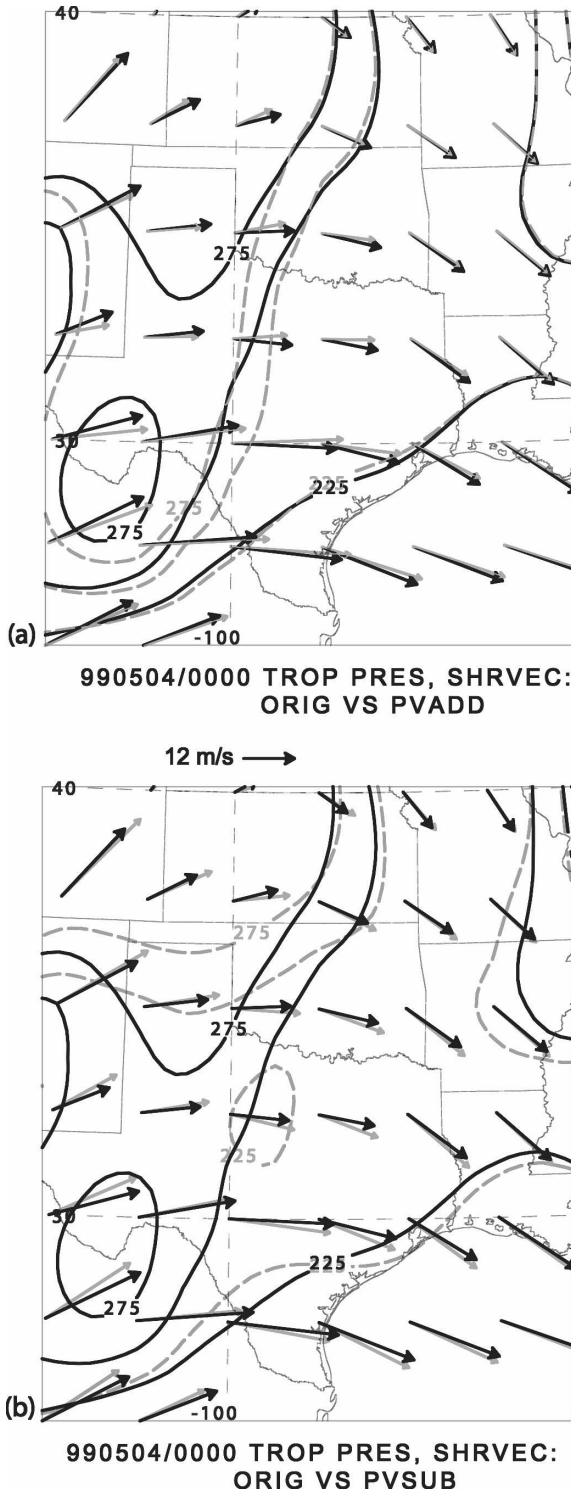


FIG. 11. Analyzed pressure (contoured every 25 hPa, black contours) on the dynamic tropopause and balanced 0–6-km shear vectors associated with the ORIG case [black arrows, $m s^{-1}$, and vector scale provided below (a)]. Also shown are tropopause pressure (gray dashed contours, same interval as ORIG) and shear vectors (gray arrows, same units and scale as ORIG) associated with (a) PVADD and (b) PVSUB.

The significant balanced CAPE increase produced by amplifying the SA (Fig. 8b) is not found in the 2XPV simulation of RSR02 (cf. RSR02, their Fig. 16). The lack of appreciable CAPE increases from the CNTL to the 2XPV model run is likely due to two modeled effects acting to offset mid- and upper-tropospheric cooling associated with the increased upper-level PV: 1) the elimination of excess CAPE via convective adjustment associated with more widespread simulated convection and 2) reduced surface heating because of increased cirrus clouds in the 2XPV simulation. These negative feedback processes (i.e., reduction of insolation associated with increased upper-tropospheric cloud cover and elimination of CAPE by convective adjustment) occur in nature and their complete omission from the balanced diagnosis represents a limitation in its accuracy. The reduction in CAPE noted in both the simulated and diagnosed NOPV scenarios reflects the absence of modeled (and likely realistic) feedbacks in an environment characterized by large-scale subsidence, leaving unopposed the deep-tropospheric warming associated with a decrease in upper-tropospheric PV (UPV) and associated balanced height rises. There is therefore the possibility that the balanced diagnosis will sometimes overemphasize the degree of destabilization associated with an increase in UPV because of a failure to account for counteracting unbalanced processes.

Figure 12, presented as an analog to Fig. 4, shows the trend in convective parameter magnitudes at three locations from 1800 to 0000 UTC for each of the three balanced states diagnosed (ORIG, PVSUB, and PVADD).

The values plotted represent horizontal averages (computed using a five grid point smoother) in grid boxes centered at the following three grid points: (35°N, 102.5°W), (35°N, 98.75°W), and (35°N, 97.5°W), denoted with the three-letter station names for Amarillo (AMA), Hobart, Oklahoma (HBR), and Oklahoma City (OKC), respectively. A comparison of Figs. 12 and 4 reveals remarkably close agreement between the average values of the convective parameters at both times for all three PV distributions. The following findings can be deduced directly from the balanced diagnosis:

- Virtual elimination of the SA increases deep-layer shear and related parameter values over the southern plains. At 0000 UTC, BRNSHR is diagnosed to increase from around 90 to 100 $m^2 s^{-2}$ at HBR (versus 117–125 $m^2 s^{-2}$ in RSR02). SREH is found to increase from 259 to 279 $m^2 s^{-2}$ (versus 265–300 $m^2 s^{-2}$ in RSR02).
- Amplifying the SA has the opposite effect on shear,

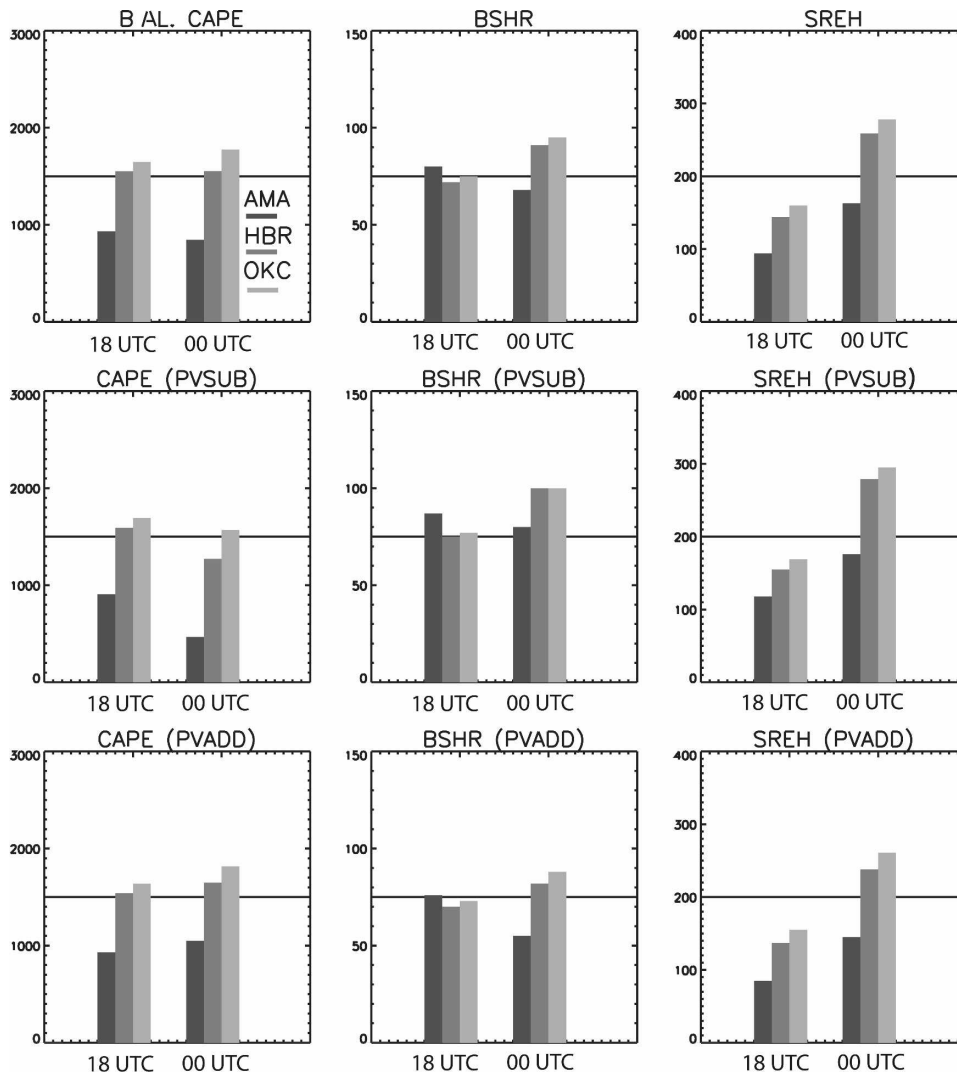


FIG. 12. Gridbox averaged values of balanced CAPE, BRNSHR, and SREH at two times, 1800 UTC 3 May and 0000 UTC 4 May 1999 for three stations (AMA, HBR, and OKC). Each row corresponds to a different balanced diagnosis (ORIG, PVSUB, and PVADD) and each column a different convective parameter. A horizontal line corresponding to half the maximum ordinate value is drawn in each panel to aid in discerning changes in the values between balanced states. This set of two time series is to be compared with Fig. 4.

reducing BRNSHR by 9 and $7 \text{ m}^2 \text{ s}^{-2}$ at HBR and OKC, respectively, and SREH by 21 and $17 \text{ m}^2 \text{ s}^{-2}$, respectively. Much more significant impacts on these two parameters were simulated by RSR02: BRNSHR and SREH reductions on the order of $20 \text{ m}^2 \text{ s}^{-2}$ and $95 \text{ m}^2 \text{ s}^{-2}$, respectively, were found in the modeled environments. It is important to note that RSR02 used the storm-motion computation methodology of Davies and Johns (1993) while we use Bunkers et al. (2000), possibly accounting for some of the difference in magnitude between their shear parameter reductions and those produced by the balanced diagnostics.

Nonetheless, the current approach correctly diagnoses the sign of the change.

- Removing the SA reduces the balanced CAPE east of the dryline (at HBR and OKC) by $200\text{--}300 \text{ J kg}^{-1}$ at 0000 UTC, identical to the simulated CAPE reduction in NOPV. Amplifying the SA increases the gridbox average balanced CAPE by 50 to 100 J kg^{-1} east of the dryline (200 J kg^{-1} at AMA at 0000 UTC), magnitudes similar to those obtained by RSR02. The absolute CAPE magnitudes computed using the reanalysis data are roughly half those observed and simulated by RSR02. This is the result of the signifi-

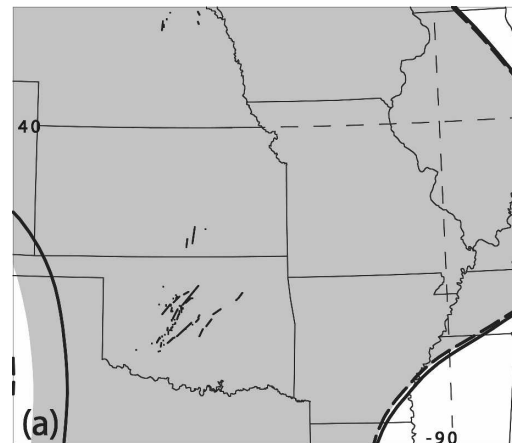
cant underestimation of surface dewpoints by the reanalysis data in this case (not shown).

The spatially averaged diagnostically computed convective parameters agree qualitatively and, to a large extent quantitatively, with those produced by the multiple-resolution modeling simulations of RSR02. This is a powerful result because it suggests that the balanced diagnostic framework is capable of explaining *how* changes in the UPV distribution regulate the convective parameter space.

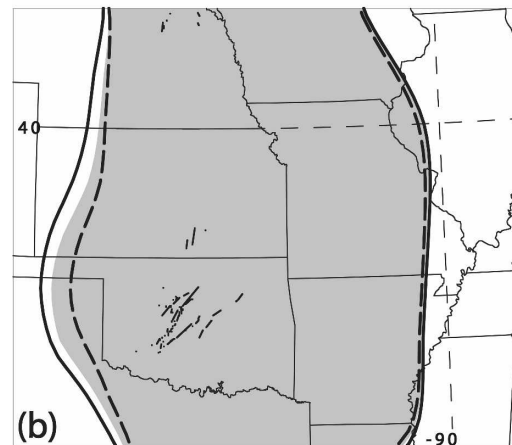
As was done for the Hesston case study in Part III, threshold contour analysis is performed below to explore the possible implications of these findings for the convective mode. Specific values of CAPE (500 J kg^{-1}), SREH ($168 \text{ m}^2 \text{ s}^{-2}$), and energy–helicity index [EHI; Rasmussen and Blanchard 1998 (hereafter RB98); 0.77] are selected on the basis of their ability to distinguish between tornadic and nonsevere convection (see Part III). Diagnosed changes in the locations of these threshold values represent possible changes in the nature of the severe weather threat there.

The threshold contour maps valid at 0000 UTC 4 May are presented in Fig. 13, with the threshold contours from the PVADD diagnosis dashed and those from the PVSUB diagnosis solid.

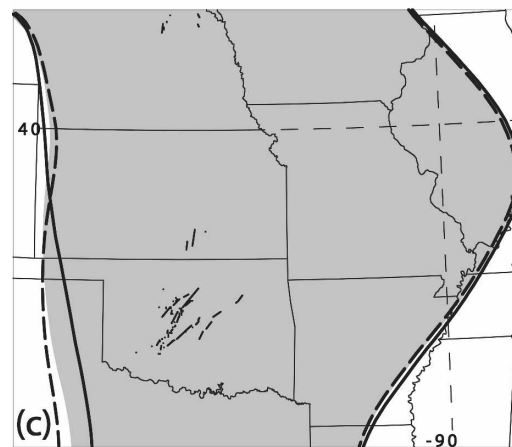
The analyzed values of CAPE, SREH, and EHI over the tornado outbreak region (central Oklahoma to southern Kansas) are all significantly higher than the threshold values of the respective parameters. Amplifying or eliminating the SA results in only small displacements of the threshold contour positions for each of the parameters, with the largest displacement apparent in the CAPE field; in the PVSUB diagnosis, the CAPE is reduced west of the outbreak area. This pushes the corresponding threshold contour eastward, about 100 km closer to the origins of the central Oklahoma tornado tracks (Fig. 13a). However, the western threshold contour for both the SREH and EHI fields, corresponding roughly to the position of the dryline, remains well to the west of the tornado tracks, suggesting that the Moore convective mode, at least as inferred from an admittedly crude analysis of the convective parameter space, is relatively insensitive to the magnitude of the SA. This finding is in broad agreement with the simulations of RSR02, which produce significant severe convection, including supercells, regardless of the initial strength of the SA. The simulation also generates a predominantly linear convective mode with a much larger areal coverage of convection in the 2XPV run, suggesting that even though the convective parameters themselves still remain well within the range supportive of supercells, a much stronger SA



990504/0000 CAPE TC



990504/0000 SREH TC



990504/0000 EHI TC

FIG. 13. Threshold contour maps for (a) CAPE, (b) SREH, and (c) EHI at 0000 UTC 4 May 1999. The shaded region encompasses all points where the analyzed parameter value is greater than the threshold contour (except for CAPE, for which the balanced values are used). The dashed and solid contours are threshold contours for PVADD and PVSUB, respectively. Tornado tracks are overplotted on (a)–(c).

could generate a squall line with more widespread convection.

5. Conclusions and implications

a. Conclusions and synthesis

A balanced diagnosis of the Moore tornado outbreak environment generally reveals the same sensitivities to selected details of the upper-tropospheric PV distribution as deduced by RSR02. The qualitative and, to an extent, quantitative agreement between these results suggests that the PV perspective can yield direct insight into the potential impact of specific PV perturbations on the convective environment. Moreover, the balanced diagnosis identifies many physical linkages between the PV perturbation of interest and the corresponding impact on the convective parameters and vertical motion field.

The PV modifications performed in the context of the RSR02 modeling study are imitated in this paper via a carefully constructed set of alterations applied directly to the analyzed PV distribution using the scheme presented in Part I. Specifically, the southern PV anomaly associated with a complex large-scale vortex emerging into the Great Plains (the SA in RSR02) is either removed or approximately doubled in amplitude, with the resulting PV anomalies inverted to compute the corresponding changes induced in the convective parameters and in the vertical motion field over the outbreak area.

As in RSR02 (their NOPV experiment), removing the SA (PVSUB) produces a concomitant decrease in the balanced CAPE within the region of modified PV, mainly along and behind the southern plains portion of the dryline. However, the CAPE increase produced by amplifying the SA (PVADD) is not noted in 2XPV, largely because of the balanced framework's omission of processes acting to counteract the increase in CAPE in both the real and modeled atmosphere. The balanced CAPE changes produced by modifying the PV in the Moore case are of identical sign and similar magnitude as those produced in the Hesston case in Part III, as well as in several other cases we have diagnosed (but not presented). Moreover, when the PV is perturbed near a background PV gradient, as is done in the Hesston case and, to a lesser extent, in the Moore case, the CAPE anomaly exhibits a spatial anisotropy such that *the CAPE perturbation is elongated in the direction roughly normal to the PV gradient*. This latter effect is absent in quasigeostrophy and is a direct consequence of using the nonlinear balance framework.

As in the Hesston case (Part III), amplifying the PV anomaly of interest (the SA in this case) increases the

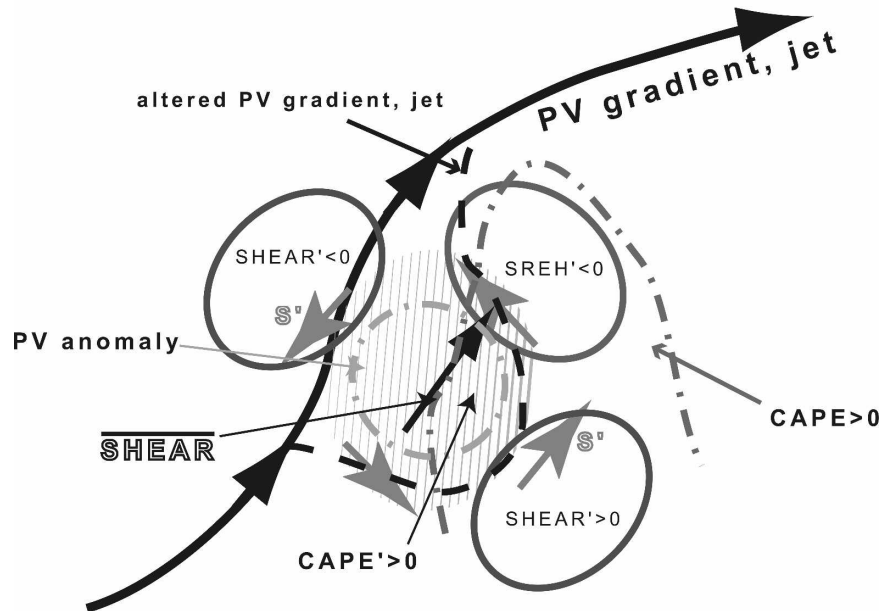
ascent downshear of the anomaly, while eliminating the SA reduces it, or even results in subsidence there. These results are in broad agreement with the RSR02 simulations, which further demonstrated that the increased (reduced) ascent downshear of the SA promoted a more (less) linear convective mode with reduced (enhanced) overall convective intensity.

Despite the use of different SMV computation methodologies, both the balanced diagnosis and RSR02 simulations produce reduced (increased) SREH and BRNSHR over the outbreak region if the SA is amplified (eliminated). The most notable difference between the two sets of results is that 2XPV reduces the shear parameters much more dramatically than does PVADD. Nonetheless, the balanced framework correctly diagnoses the sign of the SREH and BRNSHR perturbations while offering a physical explanation for the changes: amplifying the SA slightly shortens and rotates counterclockwise the deep-layer shear vector (and thus the SMV), which reduces the SREH and BRNSHR over most of the outbreak region. This differs from the explanation offered by RSR02, who attributed the shear parameter variations to changes in the way the NA and SA interact in 2XPV, NOPV, and CNTL. Balanced diagnoses of other severe convective outbreak case studies (not shown) reveal the same general response of the shear parameters to UPV modifications: *amplifying (weakening) a PV anomaly reduces (increases) the SREH downshear and on the cyclonic shear side of the anomaly, where the impact on SREH is largest. The deep-layer shear is most impacted on the anticyclonic shear side of the PV anomaly, where shear is increased (reduced) given positive (negative) PV change.*

On the basis of the results summarized above, a conceptual model relating trough amplification to changes in the convective parameters is presented in Fig. 14. The model assumes a background state typical of Great Plains convective outbreak environments (i.e., one comprising a typical southwesterly flow regime).

The figure shows the idealized spatial relationship between the background shear vector $\bar{\mathbf{S}}$ (for conceptual simplicity, assumed to be constant over the region possessing CAPE), the perturbation shear vectors attributable to a given PV amplification, and the resulting distribution of shear and SREH anomalies. For the same $\bar{\mathbf{S}}$ but oppositely signed PV perturbation (corresponding to trough removal), the sign of the shear and SREH anomalies depicted in Fig. 14 reverse but the same regions relative to the PV modification are affected. It should be emphasized that if the background shear exhibits large spatial variations across the convec-

Conceptual Model of Trough Amplification on the SCR



\overline{SHEAR} = basic-state shear vector;

S' = perturbation shear vector

— . — = PV anomaly

FIG. 14. Conceptual model schematic illustrating a circular shortwave trough (gray dashed-dotted circle) impacting the severe convective regime, defined here to be that area where $CAPE > 0$. The alteration of the PV gradient is exaggerated to clearly show the displacement of the PV gradient and jet. The hatched region is the geopotential height perturbation, elongated meridionally because of the proximity of the PV anomaly to the background PV gradient/jet. CAPE is increased over that portion of the hatched region overlapping the area where $CAPE > 0$, which itself is changed because of the CAPE increase. Total vertical shear (S) is reduced (increased) where perturbation shear ($SHEAR'$) opposes (enhances) the background shear. Storm-relative helicity ($SREH$) is reduced (enhanced) where $SHEAR'$ induces storm motion to the left (right) of the mean shear vector. Thus, $SREH$ and S are often affected in regions offset as shown. Background shear is assumed constant in the region possessing positive CAPE.

tive region, the regions of anomalous shear and $SREH$ will not be as symmetrically distributed as depicted.

A TC analysis is performed, revealing that the unperturbed Moore environment possesses so much CAPE, $SREH$, and shear that PVADD and PVSUB amount to relatively insignificant perturbations to the convective regime. In these and other case studies examined (but not shown here) where subsynoptic-scale PV changes were induced proximate to a severe storm outbreak region, *if the background environment is already favorable for significant severe convection, then subsynoptic-scale PV changes will not be able to change*

the predominant convective mode. However, this is not necessarily true near the gradients of CAPE and $SREH$, which are typically collocated with the boundaries so often directly associated with convective initiation (e.g., drylines and fronts). In these places, even relatively small changes in the convective parameters attributable to a PV change can indeed make an environment more or less supportive of supercell storms, as in the Hesston case where reductions in EHI associated with a removal of the SP reduce the EHI below the significant tornadic threshold along the Oklahoma portion of the dryline. Note that our understanding of fac-

tors governing the convective mode is far from complete, and these conclusions regarding convective mode apply to our present understanding of the importance of the convective parameter space.

b. Final remarks

One important caveat pertaining to the results obtained from the balanced diagnosis concerns the way in which the convective parameters are computed. Recently, efforts have been undertaken to refine the convective parameter climatologies performed by RB98 and others (Craven et al. 2002; Thompson et al. 2003; Markowski et al. 2003; Rasmussen 2003). These more recent studies have determined that the convective parameters formulated using the 0–1-km wind profile are most effective at distinguishing among environments supportive of significantly tornadic, weakly tornadic, and nontornadic storms when deep-layer shear is present. Specifically, the SREH computed using the 0–1-km wind profile apparently contains all of the statistically significant variance among significantly, weakly, and non-tornadic environments (Markowski et al. 2003). The current study only considered the effect of PV changes on the 0–3-km SREH; however, it is found that virtually all of the SREH change is due to changes in the SMV, with the 0–3-km wind profile itself being of secondary importance. Moreover, the 0–3-km SREH subsumes, rather than masks, the differences among storm type derived from consideration of the 0–1-km hodograph. Nonetheless, it has become evident that the details of the near-surface wind profile are very important in determining the tornadic potential, especially without the baroclinic vorticity source associated with low-level thermal boundaries. Since even strong UPV modifications apparently have little impact near the lower boundary, *it is unlikely that the subsynoptic-scale distribution of PV regulates to any significant degree the tornadic potential through its contribution to PBL winds, except to the extent that PV changes feed back on surface cyclogenesis or evolution of outflow boundaries.* In general, UPV changes will most strongly impact the winds in the upper-troposphere where the PV is being perturbed.

Another important shortcoming of the balanced diagnostic approach is that it presupposes the importance of a specific PV anomaly in governing the overall evolution of the convective regime that might, in fact, actually be more sensitive to other portions of the flow. An adjoint sensitivity analysis (Errico 1997) or similar diagnosis would lend more confidence to the assertion that a particular PV anomaly was indeed likely to be crucial to the emergence of the convective environment. For example, one could compute the sensitivity

of various convective parameters (the $J_{n,s}$ in the parlance of adjoint computations) to the details of the upper-level PV distribution at the computational cost of a single adjoint model simulation. However, the balanced diagnosis could still be used to understand how the sensitive portions of the PV field impact the convective parameters and other aspects of the environment.

The conceptual model presented in Fig. 14 provides a useful framework for qualitatively assessing the likely impact of UPV changes on the convective environment within an operational setting. The known diagnostic relationships between the PV and balanced flow variables and their spatial distribution guarantee the general applicability of the model. An important caveat in applying the conceptual model is that the SREH and vertical shear changes induced downshear of a given PV modification (northeast of the schematic anomaly embedded in southwesterly flow aloft shown in Fig. 14) will be overwhelmed by the existence of a synoptic-scale warm front, preexisting outflow boundary, or low-level cyclone, which are all associated with strongly veering low-level wind profiles and strongly enhanced SREH in that region. To apply the conceptual model to a complex situation, forecasters should diagnose changes in low-level shear and storm motion separately, and then consider the situation-specific changes in the angle between those two vectors that is so important to SREH.

The reliability and consistency of the physical relationships underpinning the conceptual model presented above crucially determine its utility to operational forecasters, not only in support of the model's general validity, but because end users will not rely on a forecasting tool or framework in which they have little confidence. RSR02 cite the lack of forecaster confidence in mesoscale model simulations as a key factor limiting the feasibility of using real-time model output in an operational environment (computational constraints notwithstanding). Thus, if a given operational forecaster is reasonably familiar with PV diagnosis, that individual will be more inclined to apply the conceptual model to a given situation and will understand the factors that limit its applicability. Use of the conceptual model relating trough structure and amplitude to the SCR will permit the forecaster to focus subsequent forecast efforts on other aspects of the environment not explained by anticipated changes in the structure and amplitude of the upper-tropospheric PV distribution.

Acknowledgments. The authors thank Christopher Davis for providing the software used in inverting the PV, as well as for providing invaluable assistance with the use of the prognostic balance equation solver. The anonymous reviewers provided many insightful sugges-

tions. This research was supported by the National Science Foundation through Grant ATM-0089906.

REFERENCES

- Bunkers, M. J., B. A. Klimowski, J. W. Zeitler, R. L. Thompson, and M. L. Weisman, 2000: Predicting supercell motion using a new hodograph technique. *Wea. Forecasting*, **15**, 61–79.
- Craven, J. P., H. E. Brooks, and J. A. Hart, 2002: Baseline climatology of sounding derived parameters associated with deep, moist convection. Preprints, *21st Conf. on Severe Local Storms*, San Antonio, TX, Amer. Meteor. Soc., 643–646.
- Davies, J. M., and R. H. Johns, 1993: Some wind and instability parameters associated with strong and violent tornadoes. 1. Wind shear and helicity. *The Tornado: Its Structure, Dynamics, Prediction, and Hazards, Geophys. Monogr.*, Vol. 79, Amer. Geophys. Union, 573–582.
- Davies-Jones, R., 1984: Streamwise vorticity: The origin of updraft rotation in supercell storms. *J. Atmos. Sci.*, **41**, 2991–3006.
- Davis, C. A., and K. A. Emanuel, 1991: Potential vorticity diagnostics of cyclogenesis. *Mon. Wea. Rev.*, **119**, 1929–1953.
- Dudhia, J., 1993: A nonhydrostatic version of the Penn State/NCAR Mesoscale Model: Validation tests and simulation of an Atlantic cyclone and cold front. *Mon. Wea. Rev.*, **121**, 1493–1513.
- Errico, R. M., 1997: What is an adjoint model? *Bull. Amer. Meteor. Soc.*, **78**, 2577–2591.
- Gold, D. A., and J. W. Nielsen-Gammon, 2008a: Potential vorticity diagnosis of the severe convective regime. Part I: Methodology. *Mon. Wea. Rev.*, **136**, 1565–1581.
- , and —, 2008b: Potential vorticity diagnosis of the severe convective regime. Part III: The Hesston tornado outbreak. *Mon. Wea. Rev.*, **136**, 1593–1611.
- Kalnay, E., and Coauthors, 1996: The NCEP/NCAR 40-Year Reanalysis Project. *Bull. Amer. Meteor. Soc.*, **77**, 437–471.
- Markowski, P. M., J. M. Straka, and E. N. Rasmussen, 2003: Tornado genesis resulting from the transport of circulation by a downdraft: Idealized numerical simulations. *J. Atmos. Sci.*, **60**, 795–823.
- Nielsen-Gammon, J. W., and D. A. Gold, 2008: Potential vorticity diagnosis of the severe convective regime. Part II: The impact of idealized PV anomalies. *Mon. Wea. Rev.*, **136**, 1582–1592.
- Rasmussen, E. N., 2003: Refined supercell and tornado forecast parameters. *Wea. Forecasting*, **18**, 530–535.
- , and D. O. Blanchard, 1998: A baseline climatology of sounding-derived supercell and tornado forecast parameters. *Wea. Forecasting*, **13**, 1148–1164.
- Roebber, P. J., D. M. Schultz, and R. Romero, 2002: Synoptic regulation of the 3 May 1999 tornado outbreak. *Wea. Forecasting*, **17**, 399–429.
- Speheger, D. A., C. A. Doswell, and G. J. Stumpf, 2002: The tornadoes of 3 May 1999: Event verification in central Oklahoma and related issues. *Wea. Forecasting*, **17**, 362–381.
- Thompson, R. L., and R. Edwards, 2000: An overview of environmental conditions and forecast implications of the 3 May 1999 tornado outbreak. *Wea. Forecasting*, **15**, 682–699.
- , —, J. A. Hart, K. L. Elmore, and P. M. Markowski, 2003: Close proximity soundings within supercell environments obtained from the rapid update cycle. *Wea. Forecasting*, **18**, 1243–1261.